Royal Netherlands
Meteorological Institute
Ministry of Infrastructure and the Environment

An improved correction method for high quality wind and temperature observations derived from Mode-S EHS

Siebren de Haan

De Bilt, 2013 | Technical report; TR-338

An Improved Correction Method for High Quality Wind and Temperature Observations derived from Mode-S EHS

Siebren de Haan

13 June 2013

Contents

Abstract

Upper air atmospheric wind and temperature information is crucial for numerical weather prediction and nowcasting. The current observation systems which are exploited to collect this information are radiosonde, aircraft, wind profilers, Doppler radar and satellites. A novel method to measure wind and temperature is related to tracking and ranging by an enhanced surveillance (EHS) Air Traffic Control (ATC) radar. This EHS radar interrogates in a selective mode (Mode-S) all aircraft in sight on which the aircraft replies with a message containing for example magnetic heading, airspeed and Mach number. From this information wind and temperature can be inferred. Since meteorological information is not directly measured in this way, preprocessing is necessary to obtain atmospheric information with adequate quality. Temperature is deduced from the Mach number and airspeed. The wind vector is deduced from the difference between the ground track vector and the orientation and speed of the aircraft relative to the air. The ground track is observed accurately but the aircraft orientation contains systematic errors and preprocessing steps are essential (de Haan, 2011). In this report the correction method is revisited taking into account the time dependency of the heading correction and, additionally, airspeed adjustment. The method developed in de Haan (2011) was limited by the fact that a heading correction value could only be estimated for aircraft regularly landing at Amsterdam Airport Schiphol. Using external sources of wind information, a heading and airspeed correction can be estimated for all aircraft when enough comparison can be generated. A dynamic heading correction database is created using the operational numerical weather prediction model from the European Center for Middle range Weather Forecast (ECMWF) and is cross validated with heading corrections derived using AMDAR wind information. This increased the number of observations by a factor of four in the Amsterdam Flight Information Region (FIR). The north-south and east-west component of wind speed observation is improved by 2 to 5% in standard deviation when both heading and airspeed corrections are applied. Next to the heading correction a flight phase dependent (ascending, descending, or constant level) temperature adjustment is developed by comparing the derived temperature against ECMWF. As it turns out, this adjustment has for some aircraft a time dependent character and thus also for this reason a dynamic temperature database has been developed. The resulting temperature bias is closer to zero, and standard deviation between model temperature and observation is reduced by 50% for all aircraft all together. For Mode-S EHS observations from AMDAR aircraft, the derived temperature observations show no improvement in standard deviation. Above 800 hPa, Mode-S EHS derived and AMDAR wind observations are comparable. Below 800 hPa, AMDAR wind observations exhibit an increase in standard deviation from 2 m/s at 800hPa to 2.5 m/s at 1000hPa when compared to ECMWF. Airspeed and heading corrected Mode-S EHS derived wind observations show to have a constant standard deviation (2 m/s) compared to ECMWF.

Chapter 1

Introduction

Nowcasting and short-range forecasting will benefit from better initialization of small scales through the assimilation of high-resolution observations. Since these small scales develop relatively fast, a high density of observations in both space and time is required. Wind observations are the most important observations for meso-scale numerical weather prediction (NWP) in order to specify the atmospheric dynamics properly. In contrast to this, high resolution upper air profile observations are lacking (Stoffelen et al., 2006; WMO, 2004, 2006)

At present, aircraft and radiosonde are the main sources of upper air wind (WMO, 2008; Cardinali et al., 2003). The radiosonde network has been optimized for beneficial impact on synoptic scales. For meso-scale meteorological applications shortcomings in the radiosonde network exist in both horizontal and temporal sampling. The horizontal sampling over land is approximately 500 km, while over the oceans only a few automatic radiosondes are launched from ships or platforms, and the temporal sampling is 6 to 12 hours. Unfortunately, the current radiosonde network is subject to reduction due to budget cuts on national levels.

The meteorological information from aircraft data used at Royal Netherlands Meteorological Institute (KNMI) is collected through the AMDAR (Aircraft Meteorological Data Relay) system supported by WMO and EUMETNET. AMDAR is the most important data source for upper air winds over the Atlantic Ocean, and the second most important data source after radiosondes over North America in the UK MetOffice model (Graham et al., 2000). Note that not all aircraft are AMDAR equipped. Benjamin et al. (1991) showed that in the Rapid Update Cycle (RUC) on a three-hour cycle from the National Centers for Environmental Prediction (NCEP) the use of aircraft data led to significant improvements in 3- and 6-h forecasts. Wind errors were reduced by approximately 10%. Moninger et al. (2003) showed that AMDAR observations improve both the short- and the long-term weather forecasts. More recent assimilation experiments showed positive short-range forecast impact in particular from aircraft observations (Benjamin et al., 2010). Assimilation experiments in the hourly RUC showed that aircraft observations had the largest overall impact on the forecast quality (de Haan and Stoffelen, 2012; de Haan, 2013). Other upper air wind information can be inferred from motion of clouds. These so-called Atmospheric Motion Vectors are used successfully in global models (Cherubini et al., 2006; Salonen and Bormann, 2011).

The error characteristics of AMDAR temperature observations have been examined in a

number of studies. A warm bias has been reported by Ballish and Kumar (2008). Drüe et al. (2007) observed aircraft type dependent systematic temperature errors. ECMWF has introduced an aircraft and flight phase dependent temperature correction Cardinali et al. (2004). In general, the standard deviation of AMDAR temperatures versus radiosonde temperature or AMDAR temperature observations very close to each other is around 0.6K (Schwartz and Benjamin, 1995; Benjamin et al., 1999). The formal error is slightly smaller, 0.4K (Painting, 2003). The error in the wind is between 2 to 3 m/s.

Only recently a method to derive wind and temperature information from all aircraft in sight of a tracking and ranging (TAR) radar has been developed (de Haan, 2011). Using the Enhanced Surveillance (EHS) data retrieved by selective mode (Mode-S) of the TAR-1 radar data of Air Traffic Control at Amsterdam Airport Schiphol, de Haan (2011) showed that the wind information that is derived from this source has a quality close to AMDAR wind observations. Temperature information can also be inferred from Mode-S EHS information, however the quality of these observations is lower than AMDAR temperature observations. The Mode-S EHS derived wind observations were successfully assimilated in a RUC model with positive impact up to 4 hours in the upper air wind forecast (de Haan and Stoffelen, 2012).

Another novel method to obtain wind and temperature information using Mode-S EHS is by exploiting other available meteorological information that can be triggered by a Mode-S EHS equipped radar, the Mode-S EHS register Meteorological Routine Air Report (Strajnar, 2012, MRAR). The wind and temperature information extracted by this system are accurate with similar quality as AMDAR for wind and temperature. A slight drawback is that only roughly 5% of all aircraft transmit the requested meteorological information.

Another interesting source for meteorological information is closely related to both Mode-S EHS, Mode-S MRAR and AMDAR. For fleet management, airlines extract all kind of information to monitor the aircraft in operation. These Automatic Dependent Surveillance Contract (ADS-C) messages contain information on the position and also on the wind and temperature. In a study on the quality on the meteorological content it was found that the quality is very good when compared to Numerical Weather Prediction (NWP) from the European Centre for Medium Range Weather Forecasting (ECMWF) (de Haan et al., 2013)

This report describes new methods to improve the quality of Mode-S EHS derived meteorological observations. The quality is assessed by comparison with ECWMF model data and AMDAR observations.

This report is organized as follows. In the next section the data used in this report is described; aircraft meteorological observations, the NWP model data from ECMWF and radar radial wind observations. Next the flight phase dependent temperature correction is presented. The heading correction methods are presented in Section 4, followed by the airspeed correction methods in Section 5 using NWP, AMDAR and weather radar radial velocity. Section 6 presents the results of all corrections.

Chapter 2

Data

This section describes the data used in this study.

2.1 Aircraft observations

Aircraft are equipped with sensors which measure (or derive) the speed of the aircraft relative to the air, its position and ambient temperature and pressure. These observations are crucial for flight safety. Wind information can be derived from these measurements. At present, a selection of these observations are transmitted to ground stations using the AMDAR (Aircraft Meteorological Data Relay) system, since not all aircraft are AMDAR equipped. An atmospheric profile can be generated when measurements are taken during take-off and landing as described in Painting (2003). Important to notice is that in general the airspeed is derived on-board from the measured (and on-board calibrated) parameters Mach-number and ambient temperature (See Appendix A).

A new type of aircraft related meteorological information stems from the observations derived from a tracking and ranging radar used for Air Traffic Control. This data is called Mode-S EHS (because it is using the selective interrogation mode of the enhanced surveillance radar). The raw flight information from Mode-S EHS retrieved by the ATC tracking radar contains information on the ground speed, track angle, magnetic heading, airspeed and Mach number. The ATC radar selectively interrogates all aircraft separately every 4.2 seconds, on which the transponder responds with sending the above mentioned parameters over a radio link to the ground. These parameters are defined by the International Civil Aviation Organization (ICAO 2007). Within European designated Mode-S EHS airspace, as is the case in France, United Kingdom and Germany, aircraft are required to disseminate this information when interrogated by a Mode-S EHS ATC radar. These messages are known as Broadcast Dependent Surveillance (BDS) and the BDS mandatory registers containing these parameters for Mode-S are BDS4,0, BDS5,0 and BDS6,0.

The difference between AMDAR and Mode-S EHS derived observations lies in the method of pre-processing to obtain wind and temperature information. AMDAR uses the on-board computer to extract the temperature information and to calculate the wind vector with an additional internal quality control step (see Painting, 2003). Mode-S EHS uses raw flight

information which is an almost direct read-out of the aircraft sensors. The pre-processing of Mode-S EHS to derive wind and temperature is performed at a ground facility.

In total four and a half year of Mode-S EHS data are used in this study. This data was collected in real time in a semi-operational manner which implies that an outage on some days occurred.

2.1.1 Observing temperature using aircraft

AMDAR (and Mode-S MRAR) temperature measurements are direct read-outs of the board-computer information. In contrast too this, Mode-S EHS temperature is derived from the Mach-number M and the airspeed v_a,

$$T_{EHS} = K \left(\frac{v_a}{M} \right)^2, \tag{2.1}$$

where K is a given constant. As was shown in de Haan (2011) the reduced measurement resolution of the Mach-number and airspeed reduces the accuracy of the derived temperature drastically. A smoothing algorithm, based on a linear approximation of the Mach-number and airspeed over 60 seconds (15 observations) centered around observation time improves the quality, but still not satisfactory when compared to the quality of the AMDAR temperature observation. An improvement in temperature can be achieved based on the knowledge that a temperature bias dependent on aircraft and phase of flight is present in AMDAR, as was shown by Cardinali et al. (2004); Drüe et al. (2007). Since Mode-S EHS exploits the same sensor this bias will be present for Mode-S EHS, as will be shown later. Applying this bias correction will be beneficial for the quality of the derived Mode-S EHS temperature observation.

2.1.2 Observing wind using aircraft

The wind vector $\mathbf{v}$ is the difference between the motion of the aircraft relative to the ground and its motion relative to the air. Thus $\mathbf{v}$ is the difference in heading vector $\mathbf{v_a}$ defined by length v_a and heading α, and the ground track vector $\mathbf{v_g}$, defined by ground speed v_g and track angle α_g, that is

$$\mathbf{v} = \mathbf{v_g} - \mathbf{v_a}. \tag{2.2}$$

The equation is correct when both angles (α and α_g) have the same reference. The Mode-S EHS heading α is not reported with respect to true north but with respect to the magnetic north. This will introduce a wind error and an additional heading correction is necessary as was explained in de Haan (2011) and is revisited in this report. An additional airspeed correction is presented as well in this report.

Table 2.1 presents the sources of information to obtain wind and temperature observations using AMDAR, Mode-S EHS and Mode-S MRAR.

Table 2.1: Summary of measured and derived meteorological parameters.

parameter	AMDAR/Mode-S MRAR	Mode-S EHS
temperature	measured	derived from Mach and v_a (on ground)
wind	derived from v_a, true heading and ground track (on-board)	derived from v_a, magnetic heading and ground track (on ground)

2.2 ECMWF

The NWP model data used in this study is obtained from the operational ECMWF model run. The output was available every 3 hours with a maximal 12 hours forecast length. The first part of the period the model version was IFS Cycle 32r3. On January 26 2010 a model upgrade was performed to Cycle 36r1. The horizontal resolution was increased from T799 to T1279 (roughly from 25km to 16km). An ECMWF wind and temperature value at a certain position and height is calculated using log-linear interpolation in the pressure, bi-linear interpolation in horizontal position and linear interpolation in time.

2.3 Radial wind measurements

A Doppler radar generally determines the radial velocity of scatters by autocorrelation of the received signal for subsequent transmitted pulses. During pulse pair processing, the velocity is effectively deduced from the phase jump of the received signal.The observations from the two Doppler radars operated by KNMI are used in this report. The combination of both radars result in a very good coverage in the Netherlands region.

Chapter 3

Temperature improvement

As was presented by de Haan (2011), a smoothing algorithm is applied to the Mach number and airspeed to improve the temperature observations derived from Mode-S EHS. In this section a flight phase, time dependent and aircraft specific temperature correction is presented. As said before, in case of Mode-S EHS temperature derivation, the temperature is derived from the Mach number and the airspeed (see Equation 2.1). The airspeed is not directly observed but is calculated using Mach number and temperature observations. Later we will see that an airspeed correction is beneficial for improved wind measurements, this correction should not be applied to recover the temperature measurement, since the actual Mach number, temperature and airspeed on-board of the aircraft are related through Equation 2.1, and the MAch number has been calculated using the (uncorrected) airspeed and temperature.

3.1 Flight phase dependent and aircraft specific temperature correction

The airflow pattern around the fuselage depends on the phase of flight (Haering, 1995). ECMWF (Cardinali et al., 2004) applies an individual correction dependent on the phase of flight of the AMDAR aircraft temperature observations. Here a similar method is applied to Mode-S EHS derived temperature. The correction values are generated by determining the difference of Mode-S EHS derived temperature observations with ECMWF temperature. Important to note is that the Mode-S EHS derived observations are not assimilated in the ECMWF model, otherwise the model could be biased towards the observations which implies that the actual offset cannot be revealed. When the observations are assimilated this problem can be avoided by using model forecast with long lead times (e.g. 24 hours). The flight phase of an aircraft is detected by inspection of the aircraft height change. When the change in height is less than 0.5 FL (1FL = 100ft $\approx$ 30m) in 4 seconds the aircraft is expected to fly at a cruise level, when the height increases with more than 0.5FL in 4 seconds the aircraft is ascending and descending when less than -0.5FL in 4 seconds. For some aircraft only cruise flight data is available because these aircraft do not operate at airports in The Netherlands or adjacent countries. Some aircraft have a constant correction over the whole period (Figure 3.1 top and bottom panel),

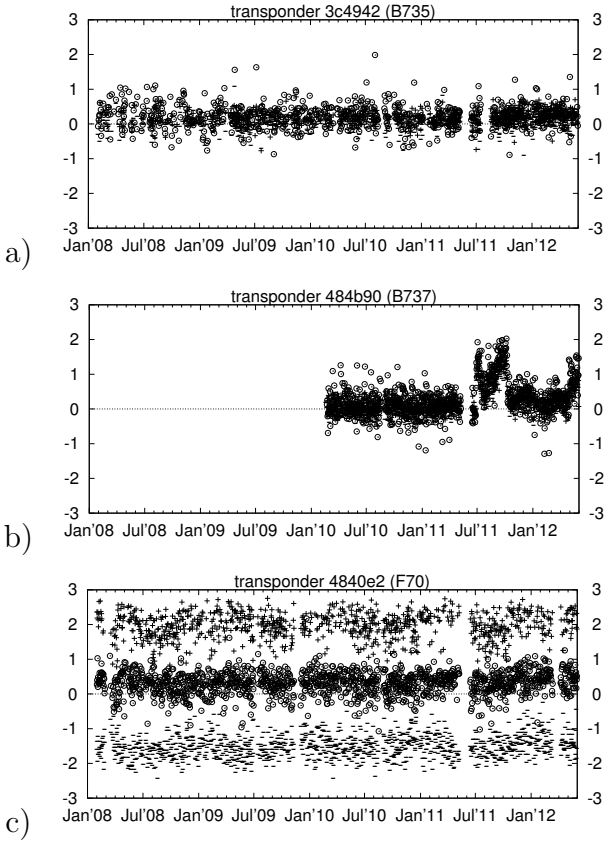

Figure 3.1: Daily ascending (+), descending (-) and level flight (o) temperature corrections for three different aircraft.

while others show a time dependency as can be seen in (Figure 3.1 middle panel). The bottom panel shows that some aircraft have clear different correction for ascending, descending and level flight (or constant flight level). For those aircraft which exhibit no jumps in the three corrections (ascending, descending and level flight for example shown in Fig. 3.2a) and c)), the mean value over the whole period is shown in Figure 3.2. The mean for level flight phase corrections is plotted in Figure 3.2 for all aircraft for which minimal 100 days of temperature corrections were recorded and the standard deviation of the temperature corrections over a single day is smaller than 1 K. From this figure one can see that there appears to be a (loose) relation of the value of the correction and the aircraft type. Furthermore, the bias of Boeing aircraft is in general slightly positive, while Airbus aircraft have level flight corrections around zero. The spread in level flight temperature correction for Boeing aircraft is slightly larger than for Airbus aircraft with some B772 and B773 having much larger spread and more negative temperature corrections. Some aircraft (e.g. CRJ's from Canadian Regional Jet) have a very small spread in level flight temperature correction.

Figure 3.3 shows the difference in temperature corrections for different flight phases. The top panel shows the level flight correction (τ^0) versus the descending correction (τ^-). Both Fokker aircraft (F50 and F100) have more negative values for descending than level flight,

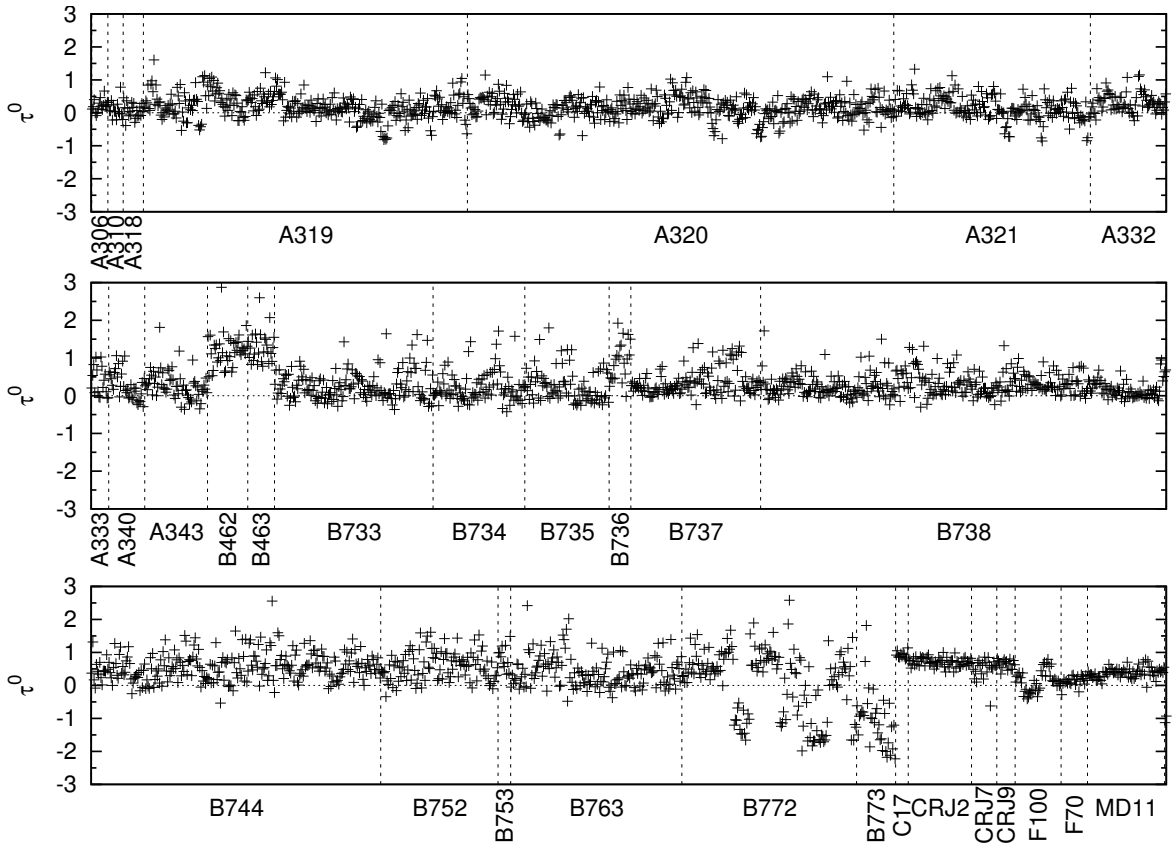

Figure 3.2: Mean level flight temperature correction τ^0 over the whole four and half year period per individual aircraft. Only those mean τ^0 are plotted for which minimal 100 days of temperature corrections were available with for each day a standard deviation of the correction which is less than 1 K.

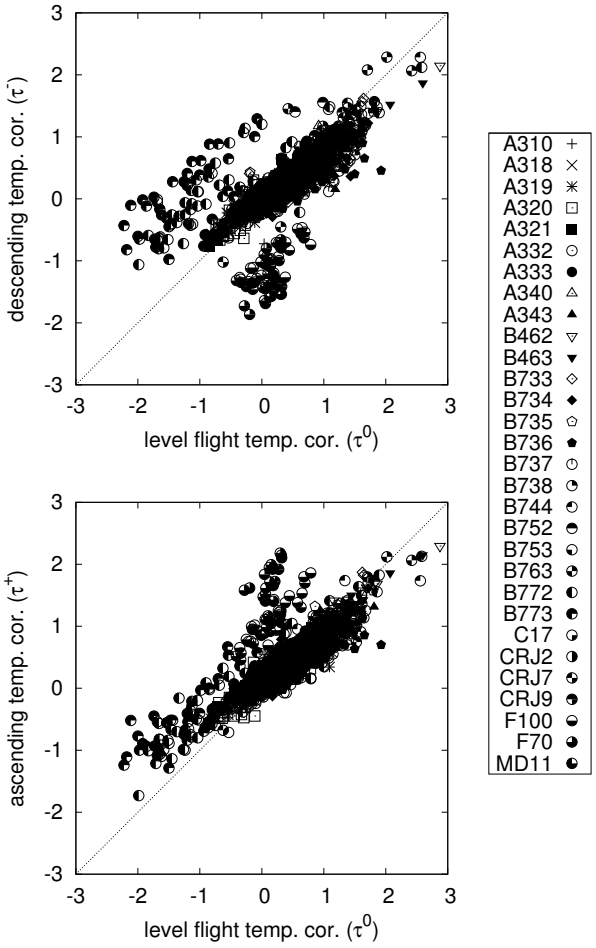

Figure 3.3: Scatter plot of level flight temperature correction (τ^0) versus descending (τ^-) temperature correction (top panel) and ascending temperature (τ^+) correction (bottom panel) for all aircraft. Only those mean τ^0 are plotted for which minimal 100 days of temperature corrections were available with for each day a standard deviation of the correction which is less than 1 K. The different symbols denote different aircraft types.

while B772 and B773 show an opposite signature. The bottom panel shows the difference between ascending (τ^+) and level flight corrections (τ^0). The majority of aircraft have nearly the same corrections for ascending and level flight. When aircraft have different corrections the ascending correction is generally higher than the level flight correction. Again F70 and F100 aircraft exhibit the largest differences.

A temperature correction lookup table is constructed with flight phase dependent, aircraft and time dependency. As is shown in Figure 3.1b), time dependency is important and therefore the mean correction value over the previous 50 days will be used to correct the temperature observation. The choice to wait for 50 days is by an educated guess.

Chapter 4

Heading correction

Currently aircraft measure heading with respect to true north. However, the Mode-S EHS BDS 5,0 messages contain the heading with respect to the magnetic North pole. The magnetic heading is not directly measured in the aircraft; magnetic variance tables are used by the aircraft inertial reference unit to convert the heading with respect to true north to magnetic heading. This will introduce errors. For example, Boeing aircraft magnetic variance tables are updated in 10-year intervals. Updating these tables is important to correct for changes in the Earths magnetic field and primarily to correct for movement of the magnetic poles (see Weinstein, 2009).

A true north heading is required to estimate the wind vector using the absolute and relative motion of an aircraft. Since the magnetic heading is reported, a correction to true north is necessary. Moreover, it is very likely that (slightly) outdated magnetic variance tables are used and thus an additional correction might be needed. Thus, the true north heading (α_t) is obtained by a correction of the reported magnetic heading (α_m) for each aircraft separately:

$$\alpha_t = \alpha_m + \alpha_c(\tau) + \Delta(\tau, \lambda, \phi), \tag{4.1}$$

where τ is the time, α_c is the heading correction to account for out-dated variance tables or other constant heading errors, and $\Delta(\tau, \lambda, \phi)$ is latitude and longitude dependent correction based on magnetic variance model defined by Maus and Macmillan (2005) (which is set to zero at Schiphol). Note that the only correction that has a position dependency is $\Delta(\tau, \lambda, \phi)$.

4.1 Estimation of heading correction

Two methods to determine the correction to the reported heading are described below. First the method exploiting landing aircraft is explained. Next, the method to determine the corrections using external wind information is presented.

4.1.1 Heading correction using landing aircraft

The size of the correction can be detected by inspecting the heading of the aircraft when it (just) has landed on the runway as has been reported earlier by de Haan (2011). When

on the runway with a significant speed, the heading of an aircraft and runway angle should match (within measurement accuracy). The method of detection requires that the position of the aircraft is on the runway and the groundspeed of the aircraft is between 55 and 120 kt (de Haan, 2011). At least three data points should meet these criteria in order to determine the mean difference between the heading and the runway angle and a minimum of 10 landings is necessary for statistical reasons. The total number of aircraft for which a landing correction is available is restricted to those aircraft which land at Amsterdam Airport Schiphol. The heading offset varies per aircraft type but may also change with time. Some aircraft types have almost no variation, while other types show a large variation. Figure 4.1 shows an example of the calculated heading correction as obtained using information during landing; the offsets are daily mean values. Clearly visible is the abrupt change for this aircraft in April 2012; a change like this might occur due to maintenance and/or updates of the magnetic variance tables.

4.1.2 Heading correction using external wind from AMDAR and ECMWF

Another method to determine the heading correction is by using external wind information and calculating backwards what the heading (and airspeed) of the aircraft should have been assuming that the external wind vector is perfect. The estimation of the true heading using an external wind vector $\mathbf{v} = (v \sin d, v \cos d)$ (wind speed v and direction d) and the given that the ground speed v_g and track angle α_g is given by

$$\tilde{\alpha}_t = \arctan\left(\frac{v_g \sin\alpha_g - v \sin d}{v_g \cos\alpha_g - v \cos d}\right). \tag{4.2}$$

The estimation of the correct heading is independent of the true airspeed of the aircraft. An airspeed adjustment will be discussed in the next section. An external wind vector will contain errors and thus influence the quality of the estimated correct heading. An estimate of the error in the heading correction is obtained by assuming the wind vector has an error in wind speed of δ_v and in wind direction of δ_d. The first order approximation for the estimated heading $\tilde{\alpha}$ is

$$\tilde{\alpha} \approx \alpha_0 + \frac{-\delta_v\, v_g \sin(d+\alpha_g) + \delta_d\,(v^2 - v v_g \cos(d+\alpha_g))}{(1+\tan^2\alpha_0)(v_g\cos\alpha_g - v\cos d)^2}, \tag{4.3}$$

where α_0 is the accurate correction. The ranges of values of the ground speed v_g, airspeed v_a, wind speed v, wind speed error δ_v and wind direction error δ_d are (based on general aircraft velocities and wind regimes)

$$v \approx 0 - 40 m/s \tag{4.4}$$

$$v_g \approx v_a \approx 100 - 250 m/s \tag{4.5}$$

$$\delta_v \approx 2 - 4 m/s \tag{4.6}$$

$$\delta_d \approx 15\,\text{deg} = \frac{\pi}{12}, \tag{4.7}$$

An upper bound of the absolute difference between the accurate and the estimated heading correction can be found by

$$\begin{aligned} |\tilde{\alpha} - \alpha_0| &\leq \frac{1}{v_a^2}\left(\delta_v v_g + \delta_d(v^2 + v_g v)\right) \\ &\approx \frac{\delta_v}{v_g} + \delta_d\left(\left(\frac{v}{v_g}\right)^2 + \frac{v}{v_g}\right) \\ &\approx \frac{\delta_v}{v_g} \approx 1 - 2\,\mathrm{deg} \end{aligned} \tag{4.8}$$

Use of a single external wind vector will be insufficient to accurately estimate the heading correction and the heading correction will be estimated using a (large) number of wind vectors.

Two sources of wind vector information are used: wind estimates from ECMWF, and wind observations from AMDAR. The benefit of using ECMWF (or NWP data in general) is that for all aircraft a heading correction can be calculated as not all aircraft are AMDAR equipped. However, there are some drawbacks for using this data source to estimate the heading corrections. It is important that the Mode-S EHS derived wind information is not used in the NWP information to avoid correlations. That is, either the Mode-S EHS derived observations are not assimilated at all, or a model forecast with sufficient lead time is used. The model used in this study had no Mode-S EHS derived data assimilated. Another issue is that using NWP data introduces an error in heading correction because the model is not perfect and has, at least, some representative errors (i.e. the model parameter represents the mean value in a 3D box).

Using wind from AMDAR results in a low number of available aircraft with an adequate heading correction since only a selected number of aircraft are AMDAR equipped. Since AMDAR aircraft are also tracked by the Air Traffic Control radar, a heading correction can be estimated for each AMDAR aircraft using the AMDAR wind which calculated on-board using the true heading. Unfortunately, the observations are not exact collocated because the observation frequencies of AMDAR and Mode-S EHS differ. Since Mode-S EHS has an observation frequency of once per four seconds the mean distance between an AMDAR and a Mode-S observation is about 10 km. This results in a (small) error in wind vector used to determine the AMDAR correction. The three heading corrections (landing, NWP and AMDAR) can be used to verify the consistency of the corrections.

Figure 4.1 shows the daily mean heading correction for a specific aircraft. The AMDAR observations were not available over the full period; the first AMDAR report was send on 2009/12/11. Clearly visible is the more smooth heading correction based on NWP wind which is related to the large number of measurements per day (over 1000 for this aircraft) compared to AMDAR (around 10 to 20 per day) and landings (between 1 and 4 per day). Also clearly visible is the sudden jump in all daily mean heading corrections on 2012/04/21 from values around 1 degrees to just below 0 degrees (no correction). Also noticeable is slight offset between AMDAR and NWP (roughly 0.5 degree). This could be related to (small) deviations in the alignment of the measurement of the true heading. Although the spread of the landing correction is larger than the NWP heading correction, the mean values do not differ for this aircraft.

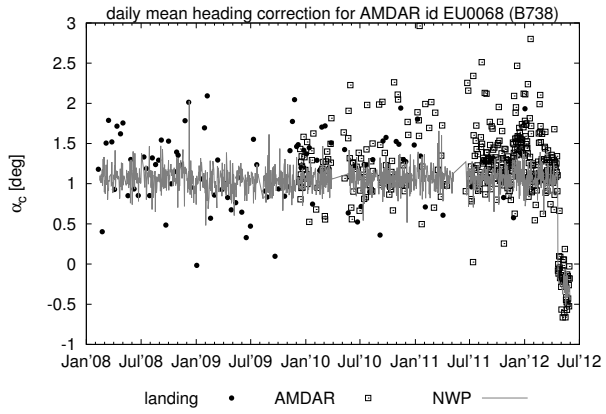

Figure 4.1: Example of different heading corrections for a specific aircraft. Dots are heading corrections obtained from landing, open squares are corrections based on AMDAR wind information and the grey lines are corrections based on NWP wind information.

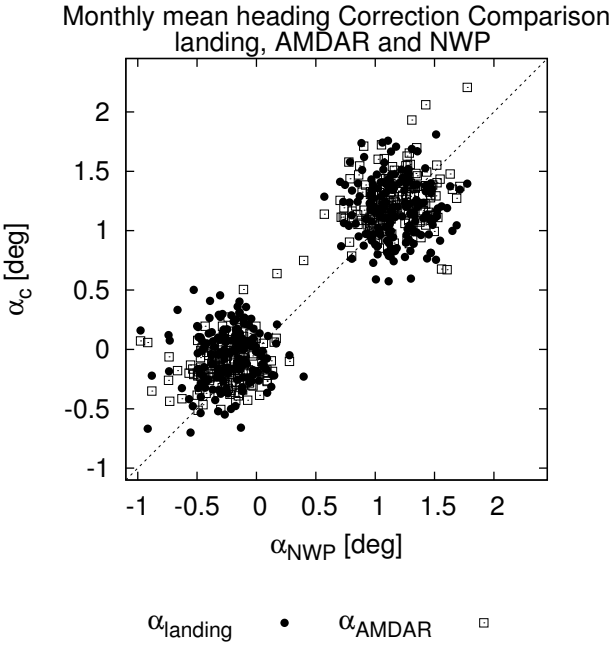

Figure 4.2: Scatter plot of NWP heading corrections (horizontal axis) versus AMDAR (open boxes) and landing heading corrections (solid circles). All three corrections are monthly averages for each individual aircraft (29) from the full four and a half year period.

Table 4.1: Number of AMDAR aircraft detected in the Netherlands airspace and number of AMDAR aircraft landing at Amsterdam Airport Schiphol. The number between brackets is the number of monthly average heading corrections per aircraft type (see text).

Aircraft type	AMDAR	landing at Schiphol
Airbus A300	2 (25)	
Airbus A319	41 (1161)	
Airbus A320	55 (1777)	
Airbus A321	72 (1933)	
Airbus A330	4 (36)	
Airbus A333	12 (172)	
Airbus A340	12 (37)	
Airbus A343	15 (81)	
Airbus A346	1 (2)	
Airbus A380	6 (16)	
Airbus A388	1 (4)	
Boeing B717	5 (59)	
Boeing B733	11 (530)	
Boeing B736	16 (408)	
Boeing B737	35 (628)	6 (63)
Boeing B738	30 (720)	17 (220)
Boeing B739	5 (141)	5 (62)
Boeing B744	21 (115)	1 (1)
Boeing B747	2 (3)	
Boeing B757	4 (22)	
Boeing B763	40 (102)	
Boeing B767	35 (84)	
Boeing B772	7 (15)	
Boeing B777	12 (91)	
Bombardier CL-600	1 (2)	
Canadair CRJ9	12 (552)	
MD11	32 (348)	
Unknown	16 (162)	

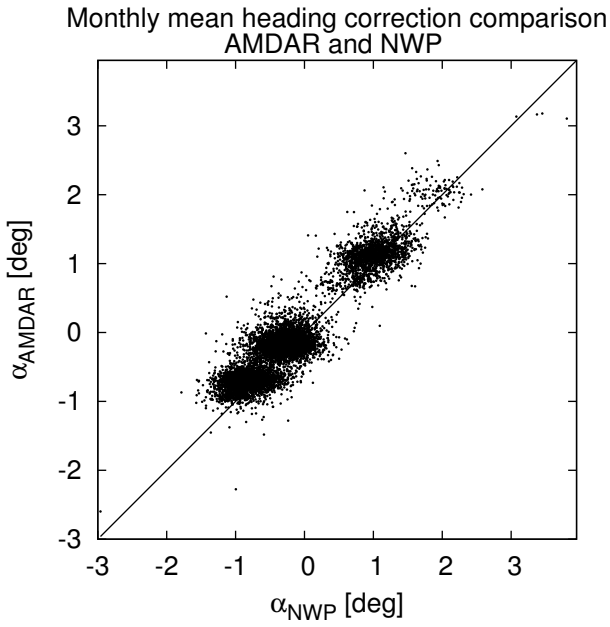

Figure 4.3: Scatter plot of all monthly mean NWP heading corrections versus the monthly mean AMDAR heading corrections (9226 points, 505 individual aircraft) for the four and a half year period.

4.2 Heading correction comparison

Figure 4.2 shows the monthly mean heading corrections for AMDAR and landing corrections versus NWP heading corrections. The magnitude of the correction is closely related to the type of aircraft, which are in this case Boeing 737, 738, 739, and 744 see Table 4.1 right column. These monthly averages compare reasonably well, that is within one degree. In total 29 different aircraft are plotted resulting in 346 monthly heading corrections. Comparing all AMDAR heading corrections with NWP heading corrections shows nearly the same signature; again the heading corrections match reasonably well. Note that more different types of aircraft are plotted in Figure 4.3 (505 unique aircraft and 9226 monthly averages from the entire four and a half year period, see Tabel 4.1). The conclusion is that the three different heading corrections are comparable within one degree, and thus an uncertainty in heading is, after correction, of the order of at most one degree.

4.3 Heading correction time dependency

The value of the heading correction for each aircraft varies with time. In de Haan (2011) is was assumed that the heading correction was constant, which was a good assumption given the data set of one year that was used. In this report a data set of four and a half year is used, and thus the time dependency may be a significant factor.

The heading correction value is determined using the NWP model comparison based on

minimal 200 observations per day. The number of 200 was chosen to have enough data to generate statistics. The mean value is calculated based on a data set over 40 days with a minimal number of 15 days of observations. The choices of these thresholds are chosen in order to have a large number of heading corrections, while being able to estimate the heading correction accurately enough. Due to several reasons mentioned before, the heading offset may change suddenly. Heading offset changes are detected by comparing the daily offset with the 40 days running mean. Absolute differences between the daily offset and the running mean which are larger than 0.5 triggers the detection of a jump in the heading correction and the heading correction is re-setted. The choice of 0.5 degree is half the expected uncertainty in the heading correction, as was derived in the previous section (see also Figures 4.2 and 4.3). Only after more than 40 days with at least 15 days of observations the running mean is reset and the heading correction value for the aircraft under consideration is used again.

4.4 Errors due to outdated magnetic variance tables

Applying a heading offset correction may introduce errors outside the area of correction since aircraft may use outdated magnetic variation tables. A simple first order correction dependent on time as presented above may therefore be only valid in the vicinity of the area for which the heading corrections were deduced (in case of NWP heading correction) or airport which was used (in case of landing heading correction). It is therefore general interest to analysis the effect of using an outdated magnetic heading correction.

Figure 4.4 shows the difference of the International Geomagnetic Reference Field (IGRF2005) model (Maus and Macmillan, 2005) between 2000 to 2014 in relation to the reference of 2010 at Amsterdam Airport Schiphol along the longitude (with latitude equal to 50 degrees North) and latitude (with longitude equal to 5 degrees East). The time dependency at Schiphol airport is removed for all years. In this way we can simulate the effect of correcting the heading with an outdated magnetic variance table with a up-to-date (landing) correction valid for Schiphol airport. As such, the figure shows the location dependent magnetic correction error due to an old magnetic variance table used in the flight management system. Assumed is that the heading correction is calibrated for the area of the Netherlands (using NWP or by the landing correction from landings at Schiphol). This implies that in the vicinity of Schiphol Airport there is no dependency on time of the correction. In the vicinity of Schiphol Airport, even with an old (say 10 years) magnetic variance table the error is small. However, for an aircraft at large distance from the Schiphol Airport the heading correction needs further adjustment. Especially, the error due to an old magnetic variance table increases more rapidly in the western direction than eastwards and also more rapidly northwards than in southward direction. The current Mode-S EHS coverage is from 1W to 8E and from 48N to 54N and this might introduce an error of at most 0.2 degrees when a 10 year old magnetic variance table is used in the flight management system to convert from true heading to magnetic heading. The value is small and thus can be neglected for the current data set. However, when Mode-S EHS observations become available from a different area this effect should be taken into account.

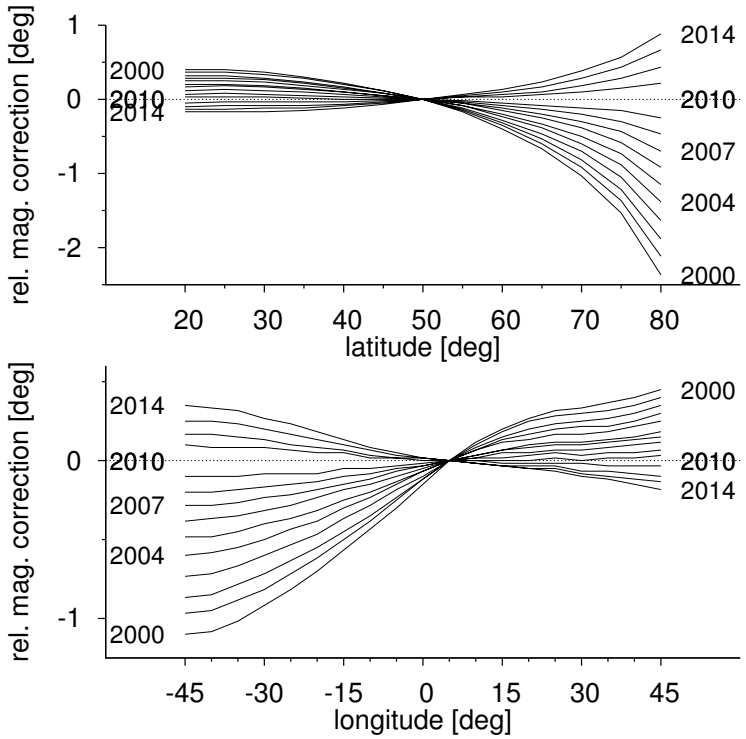

Figure 4.4: Magnetic error due to an outdated magnetic variance table, where the correct table is assumed to be from 01 Jan 2010. The toppanel shows the latitude dependence of the difference of the magnetic variance for different years relative to the magnetic variance in 2010. The bottom panel shows the longitude difference of magnetic variance. The time variability at Schiphol airport is removed, simulating a correctly estimated landing or NWP heading correction.

Chapter 5

True airspeed correction

The airspeed is determined using pitot probes (see Appendix A). Measuring the true air speed accurately is of crucial importance for flight safety. Several assumptions are made which might influence the accuracy of the measurement. For example, the mounted position of the pitot tube on the fuselage is important due to the change in flow around the aircraft during different flight phases. The Federal Aviation Administration (FAA) regulation (Piccola, 2012) prescribes correction of each system to determine the system error (that is, the relation between Indicated airspeed and calibrated airspeed) in flight and during the accelerated take-off ground run. The airspeed error of the installation, excluding the airspeed indicator instrument calibration error, may not exceed three percent or five knots, whichever is greater, throughout the speed range (Piccola, 2012).

A correction method has been developed to calibrate the airspeed which removes biases from aircraft winds. This method requires special aircraft manoeuvres by flying a wind "box" or reverse heading self-calibration (Haering, 1995; Grossman, 1977). Here a different approach is taken; auxiliary wind data is used to determine the airspeed biases.

In this section two methods of airspeed corrections are presented: an adjustment based on a linear relationship between the measured airspeed and the estimated airspeed, and a method based on a lookup table. Both adjustments, for each individual aircraft, are determined by calculating the difference between measured airspeed and estimated airspeed from the ground vector and auxiliary observation of wind information. For the linear adjustment, two sources for wind are used; the ECMWF wind and radial wind from the two operational KNMI Doppler weather radars. Note that AMDAR wind information can not be used because this information is determined using airspeed. For the adjustment using a lookup table, only ECMWF winds are used.

5.1 Linear airspeed correction

When the auxiliary wind information is a vector, both the heading and the airspeed can be estimated independently. The airspeed estimate can be determined by calculating the length

of the vector difference between the ground track vector and the wind vector, that is

$$v_a = \sqrt{v_g^2 + v^2 - 2vv_g \cos(\alpha_g - d)}. \tag{5.1}$$

The wind component along the ray from the weather radar is only known when a radial wind observation v_{rad} is used. In this case extra information is needed, such as an estimate of the heading, in order to estimate the airspeed from the ground track vector. Let $\mathbf{e_r}$ be the direction along the radar ray and $\mathbf{e_a}$ the unit heading vector (defined by heading α_t) of the aircraft and $\mathbf{v_g}$ is the ground track vector, then the airspeed can be estimated by

$$v_a = (\langle \mathbf{v_g}, \mathbf{e_r} \rangle - v_{\text{rad}}) \langle \mathbf{e_a}, \mathbf{e_r} \rangle^{-1}, \tag{5.2}$$

where $\langle , \rangle$ is the vector inner product. This equation holds when $\mathbf{e_r}$ and $\mathbf{e_a}$ are not perpendicular. Since measurements of airspeed are of crucial importance for flight safety, the actual airspeed shall not differ much from the observed airspeed. Nevertheless, an airspeed accuracy of three percent will introduce errors of nearly the same magnitude in the wind. The airspeed is initially corrected using a linear relation, given by

$$\tilde{v}_a = a + bv_a. \tag{5.3}$$

An estimate of the uncertainty for b (assuming a to be small) given the uncertainty in wind (δ_v, δ_d) is given by the first order approximation of Equation 5.1 around v_a^0,

$$v_a \approx v_a^0 + \frac{1}{v_a^0} \left(v\delta_v - \delta_v v_g \cos(\alpha_g - d) - \delta_d v v_g \sin(\alpha_g - d) \right), \tag{5.4}$$

With values of the ground speed and wind speed and direction as shown earlier, the uncertainty in the airspeed fraction can be around 0.02%. Again a single observation will not reveal the actual factor for airspeed and the mean of the ratio over a large number of points is needed.

Estimates of a and b are found for the model wind and the radar radial velocity by a least square fit per aircraft. Because the majority of observations are from overflying aircraft with airspeeds around 400 kts, airspeed range binning is necessary to obtain an estimate of the linear airspeed adjustment. Using the full data set the high airspeed values will dominate the least square fit. The mean values in each bin will be used to determine the least square fit, with a minimum of 1000 airspeed observations per bin. At least 10 bin's (each with a width of 10 kts) should be present in order to estimate a and b, in order to have a substantial range in airspeeds to perform the least squares fit. These thresholds are not fixed, others, lower or higher numbers might be used as well.

Figure 5.1 shows scatter plots of the estimates of a and b based on wind information NWP versus those based on radar radial wind. Estimates of in total 160 different aircraft are plotted with low least squares fit. The number is small due to the fact that radar radial wind observations can only be made when atmospheric scatters are present. Secondly, the upper limit aircraft which land regularly at Amsterdam Airport Schiphol is around 1500. Thirdly, the limited field of view of the radar by its horizon and range length diminishes the number of collocations, and, finally, aircraft generally avoid heavy precipitating rain clouds. The NWP

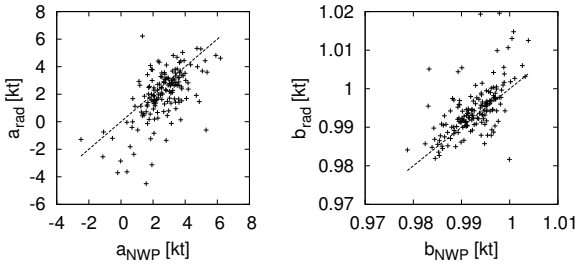

Figure 5.1: Scatter plots of coefficients a and b based on radial wind information and NWP wind information. The period runs from February 2008 to May 2012.

area is not limited and all Mode-S EHS observations can be used for the airspeed adjustment. From Figure 5.1, one can see the values of b based on radar radial wind information and NWP information correlate slightly better than those values of a. Although the airspeed estimation using radar radial winds uses auxiliary heading correction information, the estimates are similar to those when NWP wind is used in the least squares fit. All in all the correlation is rather poor due to the low number of matching observations. However, some relation between the estimates of the correction is present and it is therefore believed that the adjustment is realistic.

The observed mean airspeed correction a and b based on NWP information is plotted for each aircraft separately and is shown in Figure 5.2. The full four and a half year period is used for these estimates. From this figure it can be seen that aircraft of the same type have a similar a and b signature although the values still differ from aircraft to aircraft. For example, Airbus have a value of b close to one, while Boeing aircraft have in general a value of b slightly lower than one.

5.2 Airspeed correction using a lookup table

In general the linear adjustment of the airspeed works very well. However, Figure 5.3 shows examples were the linear adjustment fails. In this figure the mean values of the difference in measured and estimated airspeed is determined over airspeed bins of 5 kt. The figure show the six examples of large aircraft which exhibits large differences between the linear airspeed fit and the binned average values. In general, the differences are of the order of 1 kt, however as Figure 5.3f) shows there are aircraft with larger differences (upto 14 kts for an Antonov 124). Note that this is still within 3% of the true airspeed, however the difference is more than 5 kts.

Figure 5.4 shows a plot of the true airspeed correction based on the linear versus the difference between the lookup-table values and the linear fit. In general both corrections are close, however there are some extreme outliers (symbols in this figure) which relate to three of the six examples shown in Figure 5.3.

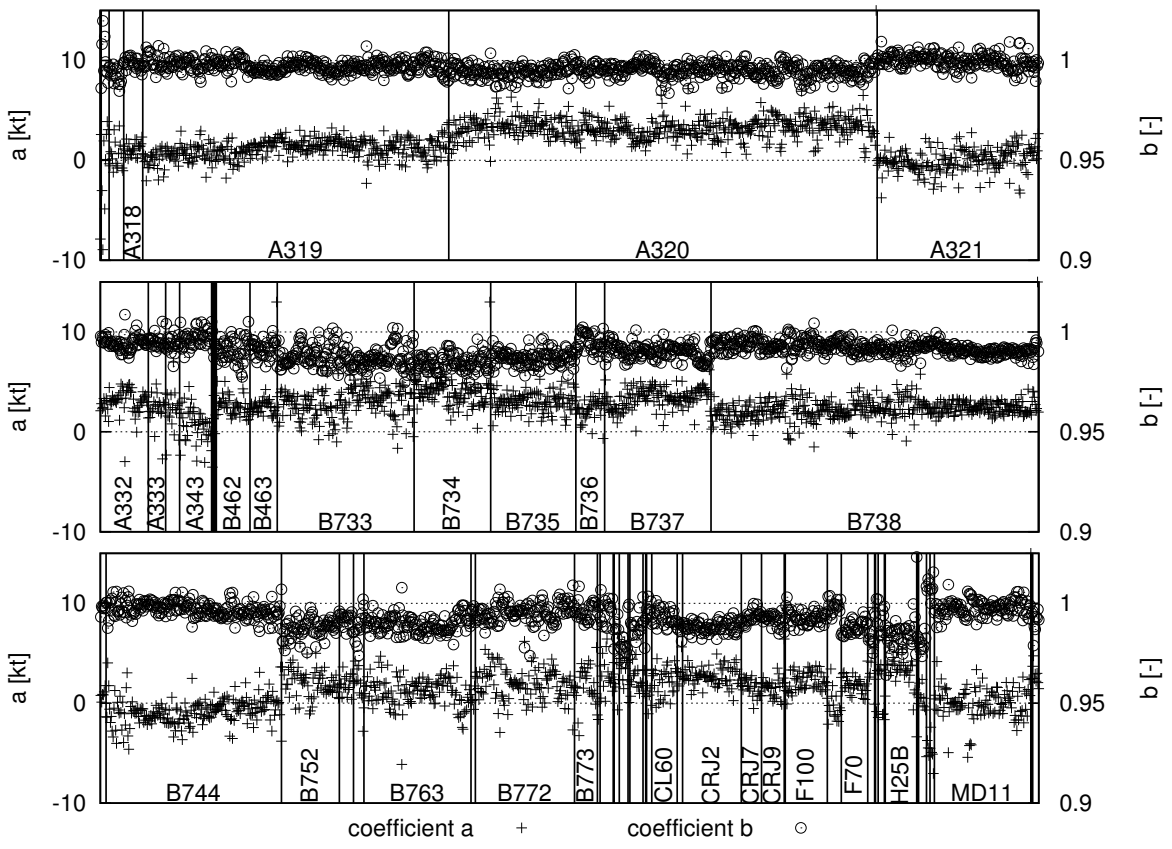

Figure 5.2: Mean values of a and b from the linear airspeed correction ($\tilde{v}_a = a + bv_a$) for each individual aircraft based on four and a half year airspeed correction values, sorted by aircraft type.

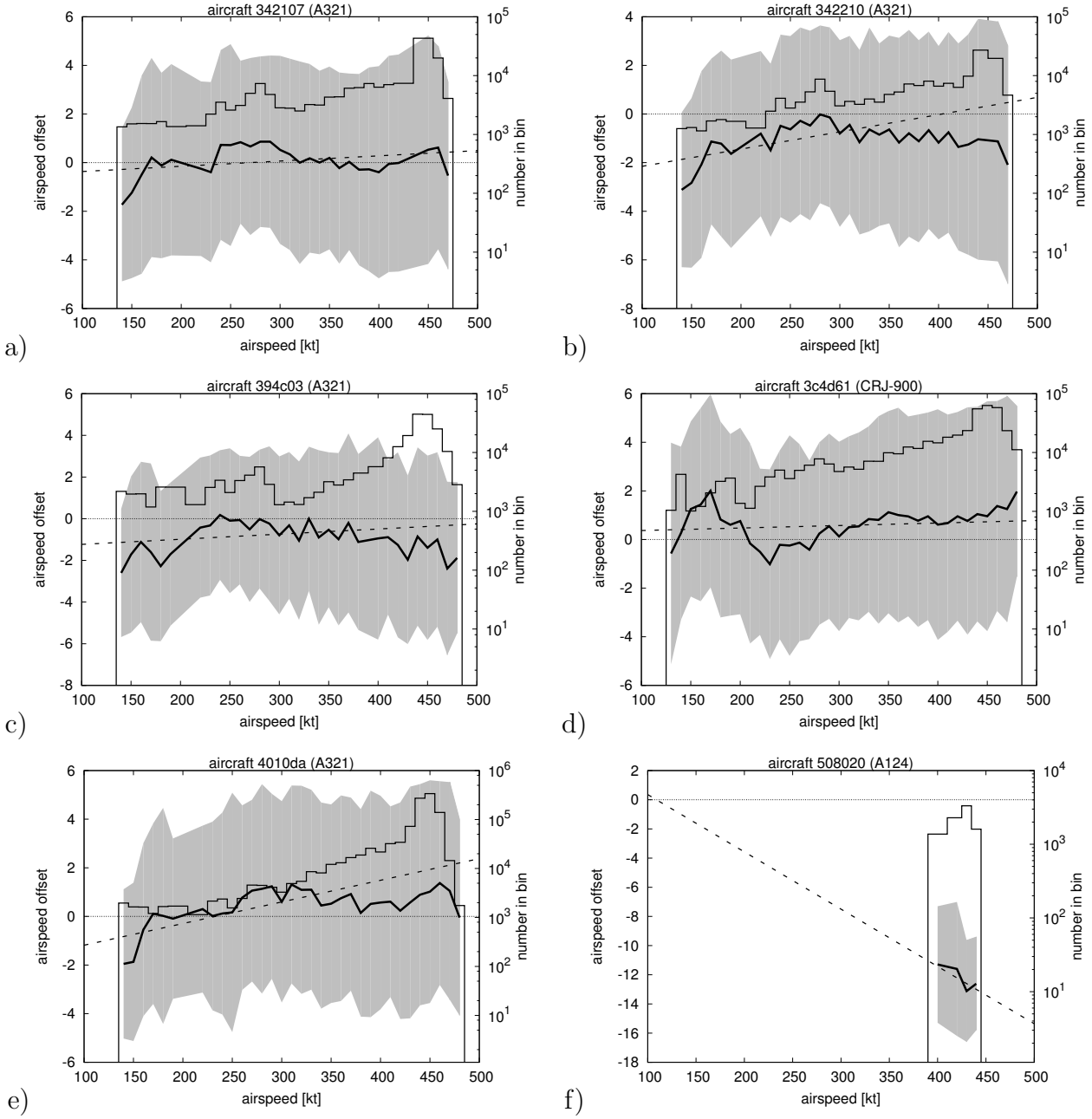

Figure 5.3: Linear fit of true airspeed offset and airspeed offset lookup table for six selected aircraft. The thick solid line shows the mean airspeed offset in 10kt bins; the shaded area represents the standard deviation in each bin; the thin solid line shows the number of points in each bin; and the dashed line shows the linear fit of the offset. Airspeed offset data is gathered over the whole four and a half year period.

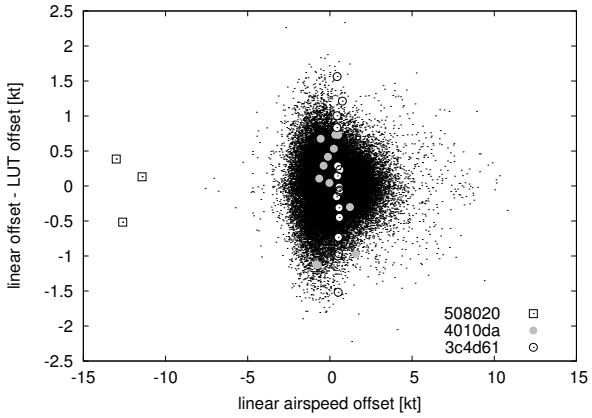

Figure 5.4: Scatter plot of the true airspeed correction using a linear fit over the whole true airspeed range against the lookup-table values. Plotted on the vertical axes is the difference between the lookup table value and the value from the linear fit. The symbols denote three of the six selected aircraft shown in Figure 5.3.

Chapter 6

Results

The number of aircraft for which proper heading corrections are available increases from around 1500 to more than 6500 (over the period February 2008 to May 2012) when NWP wind information is used instead of landing data. The increase in number of heading corrections is from aircraft which cross the Netherlands airspace regularly but do not land frequently at Amsterdam Airport Schiphol.

In this section the Mode-S EHS derived temperature and wind observations are compared to ECMWF model output and AMDAR temperature and wind observations. The effect of the different corrections (heading, airspeed and temperature correction) are shown. The observed error by comparing model and observation consists of three sources; two are related to the model and one to the observation. The observation error is related to measurement precision and techniques. The uncertainty in the model (or model error) is the sum of the forecast error and the model representativeness error. The first part of the model error has its source in (numerical) approximations of the physical laws and the uncertainty of the state of the atmosphere, while the second is due to grid approximation of the real atmosphere. The first part will grow with forecast time, while the second is constant. Note that the resolution of the ECMWF model changed during the period which might influence the statistics. The size of this effect will nevertheless be a small part of the model error.

6.1 Temperature statistics

The temperature statistics of the comparison between Mode-S EHS derived observation and ECMWF is shown in Figure 6.1. By applying the temperature correction the bias is reduced over the whole atmospheric profile. The standard deviation is also reduced but only above 800 hPa. This reduction in standard deviation is more than 50% above 700 hPa. Note that the numbers of comparison in the vertical bins exceed 10^7.

Figure 6.2 shows the comparison with ECMWF but now for matching AMDAR and Mode-S EHS derived observations. A lookup table was created which maps the transponder identifier to the AMDAR identifier and only those observations are used which were close in space and time. The maximal time difference was set to 100 seconds, the maximal horizontal difference was set to 25 km and the maximal height difference was set to 5 FL. In total 615 unique

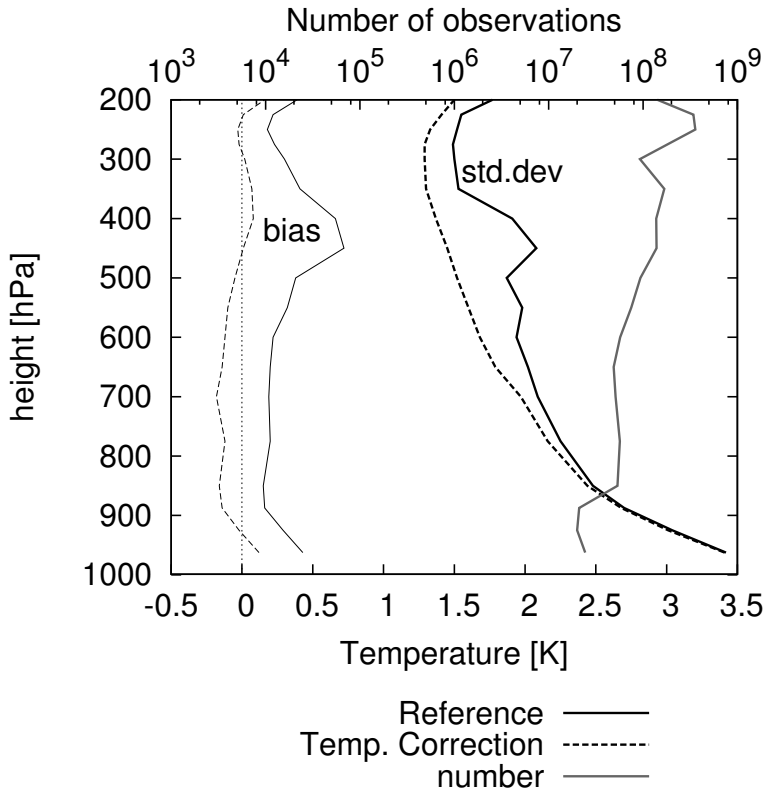

Figure 6.1: Temperature mean difference between ECMWF and observation and standard deviation of the difference for all quality controlled Mode-S EHS aircraft observations for which a temperature correction is available. The reference (no correction) is depicted as a solid black line (thin is bias, thick is standard deviation). The dashed line shows the bias and standard deviation for temperature corrected observations. The number is shown by the gray line (top axis).

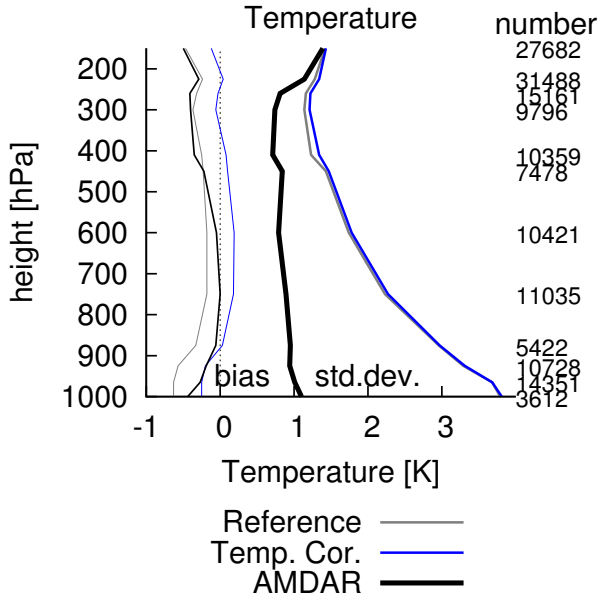

Figure 6.2: Statistics of co-located AMDAR and Mode-S EHS temperature observations with ECMWF NWP temperature data over the whole four and half year period. In gray is the uncorrected Mode-S EHS (reference), the thin blue line is the temperature corrected Mode-S EHS and in thick black line the AMDAR.

AMDAR aircraft were used in the statistics, some of them never landing at Amsterdam Airport Schiphol. In total 157 533 observations matched the above criteria. The AMDAR temperature has a constant standard deviation of 1 K but exhibits a bias of the order of around 0.5 K (in agreement with Schwartz and Benjamin (1995); Benjamin et al. (1999); Cardinali et al. (2004); Ballish and Kumar (2008); de Haan (2011). The Mode-S EHS exhibit a temperature error, after correction, of more than 3 K near the surface and 1.5 K at 300 hPa.

6.2 Longitudinal and Transversal components

Since the magnitude of the airspeed determines the longitudinal component (with respect to the aircraft orientation) of the wind vector, the airspeed adjustment will only influence this component and leave the transversal part of the wind vector unattached. Figure 6.3 shows the mean difference between observed and NWP longitudinal and transversal wind components without the airspeed adjustment and with the airspeed adjustment. In the longitudinal direction, both the mean difference between observation and model and the standard deviation are reduced. The mean difference, which was negative at the surface and positive at 200hPa has become almost zero, apart from the lowest levels (below 850hPa) and the top level (above 200hPa). The standard deviation is reduced over almost the entire profile; the reduction is of the order of 5% at 200hPa. As expected, the transversal wind component statistics do not change. Note the opposite biases in the surface layer; the cause for this is still unknown.

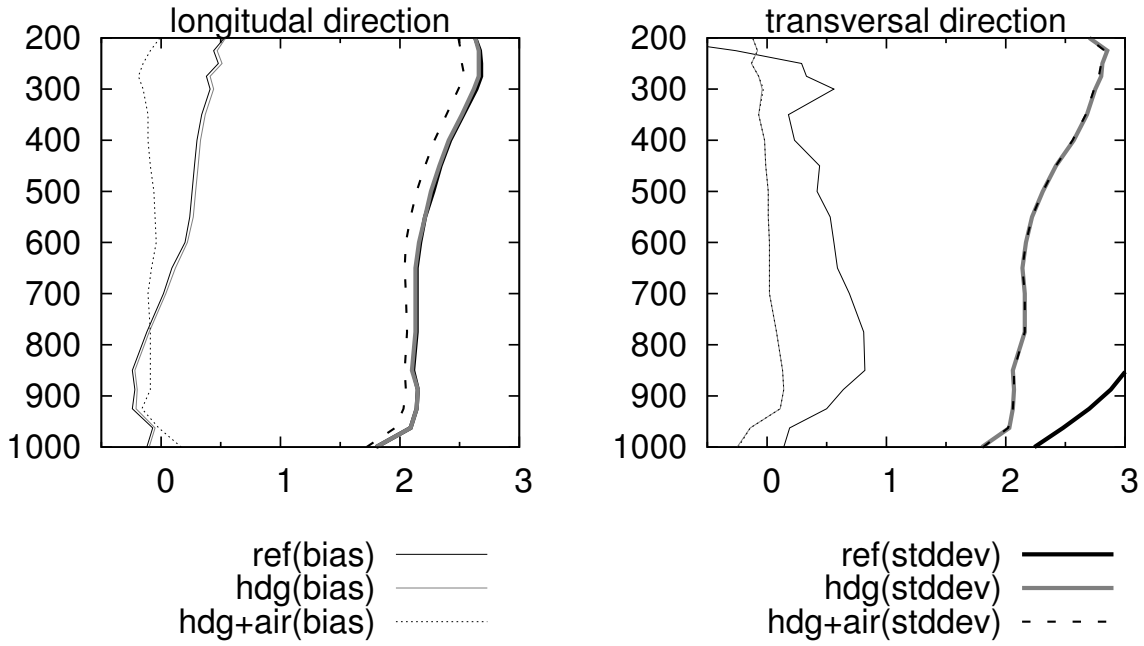

Figure 6.3: Improvement of the wind measurement statistics in longitudinal and transversal direction with respect to the aircraft axis. Black solid line is the reference, gray line is wind with only heading correction and the dashed line represents heading and airspeed correction.

6.3 Wind statistics

Figure 6.4 shows the comparison of the Mode-S EHS derived wind components against ECMWF for the whole four and a half year period. The largest improvement is observed when the heading and airspeed corrections are applied together in the u component of the wind. Over the full vertical profile an improvement of around 5% in wind speed is observed, while the bias is reduced. An improvement in v is also observed, being around 1 to 2% in standard deviation. The impact on u is not surprising since the major flying routes are directed East-West and because the airspeed corrections improves the longitudinal component of the wind.

The comparison with matching AMDAR and Mode-S EHS derived observations is shown in Figure 6.5. The u- or east-west-component of the wind is shown in the left panel. As for all Mode-S EHS derived observations, the bias for this wind component is close to zero when a heading and airspeed correction is applied. The AMDAR wind observations, however show a clear bias below 800 hPa. Also the standard deviation increases in the lower part of the atmospheric profile for AMDAR (from 2 m/s to 2.5 m/s). This behaviour of the standard deviation of AMDAR wind observations is also observed for the north-south (or v) component of the wind. The bias for Mode-S EHS derived observations of this wind component has a maximum at approximately 900hPa. AMDAR shows a similar feature but more centred around zero. At higher altitudes AMDAR wind has a negative bias, while the heading and airspeed corrected Mode-S EHS derived observations have a bias closer to zero.

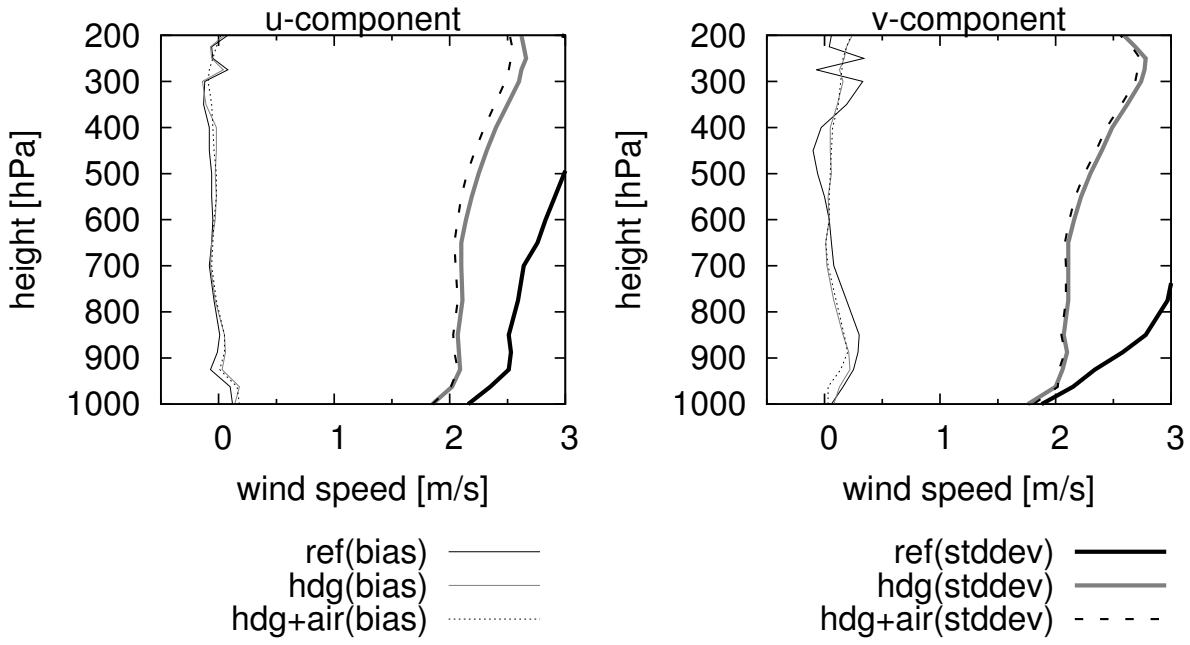

Figure 6.4: Improvement in u and v wind components. Black solid line is the reference, the gray line is wind with only heading correction and the dashed line represents heading and airspeed correction.

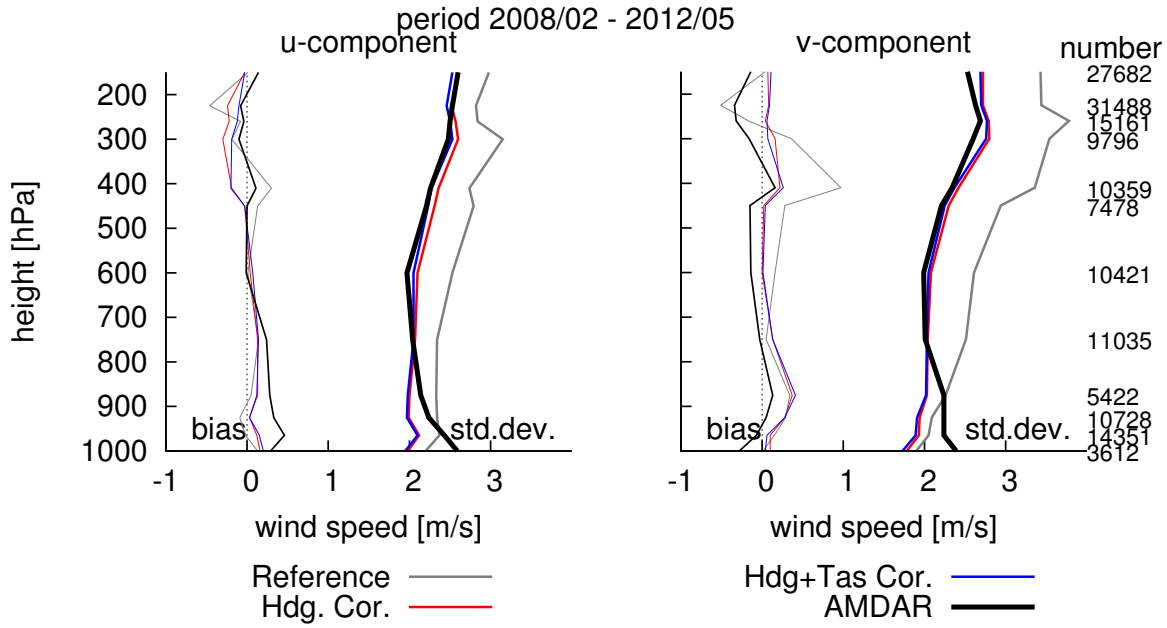

Figure 6.5: Statistics of co-located AMDAR and Mode-S EHS derived wind observations with ECMWF NWP wind data over a four and half year period. The gray line denotes the uncorrected Mode-S EHS derived observations; the red line represents the heading corrected; the blue line represents the heading and airspeed corrected and in black the AMDAR wind observation statistics.

Chapter 7

Conclusions and Recommendations

In this report the correction method as presented by de Haan (2011) for Mode-S EHS derived wind and temperature observations is revised and improved considerably. The use of NWP data to determine the heading and airspeed correction not only increased the number of aircraft for which an correction could be applied by a factor of 4, it also opened the possibility to perform airspeed and additionally temperature corrections on top of the heading correction.

The NWP heading correction for each individual aircraft is almost identical to the landing correction developed earlier with the benefit that heading deviations can be computed for all aircraft operating in the Netherlands airspace. The heading correction values showed a clear time dependency for specific aircraft, implying that a time dependent heading correction is necessary. Furthermore, as it turns out, the temperature correction requires an aircraft flight phase dependent correction, as well as a time dependent correction.

The developed corrections were applied on a four and half year Mode-S EHS data set and the resulting wind and temperature observations were compared to the ECMWF operational model data.

The introduction of airspeed correction resulted in an improved wind observation with a reduction of 5% in wind speed error in the flight direction of the aircraft. By applying the airspeed correction, the wind bias is almost zero in this direction, while the heading correction reduces bias and standard deviation in the transversal direction. The improvement in the standard deviation of the wind observation in the north-south and east-west component is respectively 5% and 2%.

The corrected temperature observations showed an almost zero bias and an improvement of the temperature standard deviation by 50% above 750hPa.

Comparing co-located AMDAR and Mode-S EHS derived wind and temperature observations showed that the standard deviation of Mode-S EHS derived wind is equal to AMDAR above 800 hPa. Below 800 hPa the standard deviation of AMDAR increases from 2 m/s to 2.5 m/s at the surface, while the Mode-S EHS derived wind standard deviation is constant and equal to 2 m/s. The temperature observation from AMDAR have a clear better standard deviation of 1 K, although the quality of the Mode-S EHS derived and AMDAR temperature observations at the 200 hPa are almost similar. Note that the AMDAR temperature observations require also an aircraft flight phase dependent correction.

The overall conclusion is that NWP derived heading, airspeed and temperature correction improve the Mode-S EHS derived observations substantially. The quality of the Mode-S EHS derived temperature is clearly less than the AMDAR temperature. However, the Mode-S EHS derived wind observation is equal to the AMDAR wind. It looks like that the derived wind information from Mode-S EHS below 800hPa is better than the AMDAR wind. The last statement needs to be confirmed with additional research with an independent wind source. Furthermore, the bias in v in the boundary needs further investigation.

7.1 Recommendations

The airspeed correction could (theoretically) also be applied to AMDAR, Mode-S MRAR and ADS-C aircraft observations, as these are derived using (uncorrected) airspeed measurements. This will improve the quality of these observations. This possibility should be considered.

Since the measurement of airspeed is crucial for flight safety, the airspeed correction and heading correction might be of interest to air traffic organizations, oversight authorities, aircraft manufacturers and airline companies.

The above presented corrections for heading, airspeed and temperature should be implemented in the processing chain of Mode-S EHS.

Acknowledgment

This study is partially funded by the Knowledge and Development Centre Mainport Schiphol in The Netherlands (KDC, http://www.kdc-mainport.nl). The author thanks Air Traffic Control The Netherlands (LVNL) for the provision of the raw Mode-S EHS data. The careful proof-reading of this manuscript by Mr Jan Sondij (KNMI) was highly appreciated.

Bibliography

Ballish, B. A., and K. V. Kumar, 2008: Systematic Differences in Aircraft and Radiosonde Temperatures, *Bull. Amer. Meteor. Soc.*, **89**, 1689–1707.

Benjamin, S. G., and K.A. Brewster, and R. Brummer, and B. F. Jewett, and T. W. Schlatter, and T. L. Smith, and P. A. Stamus, 1991: An Isentropic Three-Hourly Data Assimilation System Using ACARS Aircraft Observations, *Monthly Weather Review*, **119**, 888–906.

Benjamin, S. G., and B. E. Schwartz, and R. E. Cole, 1999: Accuracy of acars wind and temperature observations determined by collocation, *Weather and Forecasting*, **14**, 1032–1038.

Benjamin, S. G., and B. D. Jamison, and W. R. Moninger, and S. R. Sahm, and B. E. Schwartz, and T. W. Schlatter, 2010: Relative short-range forecast impact from aircraft, profiler, radiosonde, VAD, GPS-PW, METAR and mesonet observations via the RUC hourly assimilation cycle, *Monthly Weather Review*, **138**, 1319 – 1343.

Cardinali, C., and L. Isaksen, and E. Andersson, 2003: Use and Impact of Automated Aircraft Data in a Global 4DVAR Data Assimilation System, *Monthly Weather Review*, **131**, 1865–1877.

Cardinali, C., and L. Rukhovets, and J. Tenenbaum, 2004: Jet Stream Analysis and Forecast Errors Using GADS Aircraft Observations in the DAO, ECMWF, and NCEP Models, *Monthly Weather Review*, **132**, 764–779.

Cherubini, T., and S. Businger, and C. Velden, and R. Ogasawara, 2006: The Impact of Satellite-Derived Atmospheric Motion Vectors on Mesoscale Forecasts over Hawaii*, *Mon. Wea. Rev.*, **134**, 2009–2020, `http://dx.doi.org/10.1175/MWR3163.1`.

Drüe, C., and W. Frey, and A. Hoff, and Th. Hauf, 2007: Aircraft type-specific errors in AMDAR weather reports from commercial aircraft, *Q. J. Roy. Met. Soc.*, **134**, 229–239.

Graham, R. J., and S. R. Anderson, and M. J. Bader, 2000: The relative utility of current observation systems to global-scale NWP forecasts, *Quarterly Journal of the Royal Meteorological Society*, **126**, 2435–2460.

Grossman, R. L., 1977: A Procedure for the Correction of Biases in Winds Measured from Aircraft, *J. Appl. Meteor.*, **16**, 654–658.

Haan, S. de, 2011: High-resolution wind and temperature observations from aircraft tracked by Mode-S air traffic control radar, *J. Geophys. Res.*, **116**, D10111–.

Haan, S. de, 2013: Assimilation of GNSS ZTD and radar radial velocity for the benefit of very-short-range regional weather forecasts, *Quarterly Journal of the Royal Meteorological Society*, n/a–n/a, ISSN 1477-870X, http://dx.doi.org/10.1002/qj.2087.

Haan, S. de, and A. Stoffelen, 2012: Assimilation of High-Resolution Mode-S Wind and Temperature Observations in a Regional NWP model, *Weath. Forec.*, **27**, 918–937, http://dx.doi.org/10.1175/WAF-D-11-00088.1.

Haan, S. de, and L. J. Bailey, and J. E. Können, 2013: Quality assessment of Automatic Dependent Surveillance Contract (ADS-C) wind and temperature observation from commercial aircraft, *Atmospheric Measurement Techniques*, **6**, 199–206, http://www.atmos-meas-tech.net/6/199/2013/.

Haering, E. A., December 1995: Airdata measurement and calibration, *NASA Technical Memorandum 104316*, National Aeronautics and Space Administration.

Maus, S., and S. Macmillan, 2005: 10th Generation International Geomagnetic Reference Field, *Eos Trans. AGU*, **86**.

Moninger, W. R., and R. D. Mamrosh, and P. M. Pauley, 2003: Automated Meteorological Reports from Commercial Aircraft, *Bulletin of the American Meteorological Society*, **84**, 203–216.

Painting, J. D., 2003: WMO AMDAR reference manual, *WMO-no.958*, WMO, Geneva, http://www.wmo.int.

Piccola, John, 2012: Flight test guide for certification of transport category airplanes, *Technical report*, FAA, http://www.faa.gov/documentLibrary/media/Advisory_Circular/AC%2025-7C%20.pdf , last accessed: 31/01/2013.

Salonen, K., and N. Bormann, 2011: Atmospheric motion vector observations in the ECMWF system, *1-year report, EUMETSAT/ECMWF Fellowship Programme Research Report 23*, ECMWF, http://www.ecmwf.int/publications/library/do/references/show?id=90279.

Schwartz, B. E., and S. G. Benjamin, 1995: A Comparison of Temperature and Wind Measurements from ACARS-Equipped Aircraft and Rawinsondes, *Weather and Forecasting*, **10**, 528–544.

Stoffelen, A., and M. Bonavita, and J. Eyre, and M. Goldberg, and H. Järvinen, and C. Serio, and J.-N. Thépaut, and V. Wulfmeyer, 2006: Developments on atmospheric sounding and wind profiling, *Position paper - post-eps*, EUMETSAT, http://www.eumetsat.int/groups/pps/documents/document/pdf_peps_pp_atmos_sound_wind.pdf.

Strajnar, B., 2012: Validation of mode-s meteorological routine air report aircraft observations, *Journal of Geophysical Research: Atmospheres*, **117**, ISSN 2156-2202, http://dx.doi.org/10.1029/2012JD018315.

WMO, , 2004: Statement of guidance regarding how well satellites and in situ sensor capabilities meet WMO user requirements in several application areas, *WMO- TD No. 1052*, WMO, Geneva, http://www.wmo.int.

WMO, , 2006: Implementation plan for the evolution of space and surface-based sub-systems of the GOS, *WMO- TD No. 1267*, WMO, Geneva, http://www.wmo.int.

WMO, , 19-21 May 2008: Fourth WMO workshop on the impact of various observing systems on NWP, *Technical report*, WMO, http://www.wmo.ch/pages/prog/www/OSY/Reports/NWP-4_Geneva2008_index.html.

Weinstein, B., 2009: Correcting the effects of magnetic variation, *AERO Magazine Boeing Commercial Airplanes*, 15–19, http://www.boeing.com/commercial/aeromagazine/articles/qtr_04_09/pdfs/AERO_Q409.pdf.

Appendix A

Pitot measurement

Bernoulli's equation (for compressible flows at constant flight level) is constant along streamlines, that is

$$\frac{v^2}{2} + \int \frac{dp}{\rho} = C \tag{A.1}$$

Assume isentropic flow, that is

$$p = B\rho^\gamma. \tag{A.2}$$

Then

$$\frac{v^2}{2} + \int \frac{dp}{\rho} = \frac{v^2}{2} + \int \frac{dp}{Bp^{1/\gamma}} = \frac{v^2}{2} + \frac{\gamma}{\gamma - 1}\frac{p}{\rho} = C \tag{A.3}$$

We observe the static pressure p_S (and $v_S = 0$) and dynamic pressure p_T. Then, using adiabatic isentropic flow, $p_T/p_S = (\rho_T/\rho_S)^\gamma$,

$$\begin{aligned}
\frac{v^2}{2} + \frac{\gamma}{\gamma - 1}\frac{p_T}{\rho_T} &= \frac{\gamma}{\gamma - 1}\frac{p_S}{\rho_S} && \text{(A.4)}\\
\iff \left(\gamma\frac{M^2}{2} + \frac{\gamma}{\gamma - 1}\right)\frac{p_T}{\rho_T} &= \frac{\gamma}{\gamma - 1}\frac{p_S}{\rho_S} && \text{(A.5)}\\
\iff \left(\frac{M^2}{2} + \frac{1}{\gamma - 1}\right) &= \frac{1}{\gamma - 1}\frac{p_S}{\rho_S}\frac{\rho_T}{p_T} && \text{(A.6)}\\
&= \frac{1}{\gamma - 1}\frac{p_S}{p_T}^{1-\frac{1}{\gamma}} && \text{(A.7)}
\end{aligned}$$

A.1 Measurement of air temperature

$$\frac{v^2}{2} + \frac{\gamma}{\gamma - 1}\frac{p}{\rho} = C \tag{A.8}$$

$$p = \rho RT \tag{A.9}$$

T_a air temperature, T_1 stagnation temperature

$$\frac{v^2}{2} + \frac{\gamma}{\gamma - 1} R T_1 = \frac{\gamma}{\gamma - 1} R T_a \tag{A.10}$$

$$\iff \frac{\gamma - 1}{2} \frac{v^2}{\gamma R T_1} + 1 = \frac{T_a}{T_1} \tag{A.11}$$

$$\iff \frac{\gamma - 1}{2} M^2 + 1 = \frac{T_a}{T_1} \tag{A.12}$$

$$\lambda \frac{\gamma - 1}{2} M^2 + 1 = \frac{T_a}{T_1}, \tag{A.13}$$

or

$$T_a = T_1 \left(\lambda \frac{\gamma - 1}{2} M^2 + 1 \right). \tag{A.14}$$

A.2 Measurement of true airspeed

For high speed flights, v_a can be calculated as a function of Mach number and (static) air temperature:

$$v_a = M \sqrt{\frac{\gamma p_0}{\rho_0} \frac{T_a}{T_0}} \tag{A.15}$$

where p_0 and ρ_0 are the pressure and density at standard sea level, T_a is static air temperature in kelvin, T_0 is the temperature at standard sea level (288.15 K)

$$v_a = \sqrt{\frac{\gamma p_0}{\rho_0} \frac{2}{\gamma - 1} \frac{T}{T_0} \left(\left(\frac{p_T}{p_S} + 1 \right)^{(\gamma - 1)/\gamma} - 1 \right)} \tag{A.16}$$

The v_a is calibrated for position and aircraft fuselage specific effects.

Appendix B

Processing settings

B.1 Quality checks

Quality checks are performed on the Mode-S EHS parameters.

$$M > 0 \text{ [-]} \tag{B.1}$$
$$50 < v_g < 850 \text{ [kt]} \tag{B.2}$$
$$100 < v_a < 570 \text{ [kt]} \tag{B.3}$$
$$|\alpha_g - \alpha_t| < 45 \text{ [deg]} \tag{B.4}$$
$$|\alpha_r| < 2.5 \text{ [deg]} \tag{B.5}$$
$$T_{EHS} < 100 \text{ [}^o\text{C]} \tag{B.6}$$

B.2 Correction algorithm settings

B.2.1 Temperature

Temperature corrections are determined dynamically (wrt. time) for each aircraft individually.

- Ascending : $\delta FL > 0.5$ in 4.2s
- Flight level : $|\delta FL| < 0.5$ in 4.2s
- Descending : $\delta FL < -0.5$ in 4.2s
- daily averages
- minimal 200 observations per day
- τ is determined using a moving window mean value over 50 days

B.2.2 Heading

Heading corrections are determined dynamically (wrt. time) for each aircraft individually.

- daily averages
- minimal 200 observations per day
- moving window average length : 40 days
- minimal number of days with averages: 15 days
- heading correction is re-setted when
  - less than 15 daily averages in 40 days, or
  - daily average differs more than 0.5 def from moving window average

B.2.3 Airspeed

Airspeed corrections are determined for each aircraft individually.

- airspeed correction is dependent on the observed airspeed
- correction values are binned in 10 kt bins
- minimal 1000 observations in each bin
- standard deviation in the bin should be smaller than 5 kt

Appendix C

Used symbols

α_t	true heading
α_m	magnetic heading
α_g	ground track angle
α_r	roll angle
α_c	heading correction
α_{AMDAR}	heading correction from AMDAR wind
α_{NWP}	heading correction from NWP wind
α_{landing}	heading correction from landing aircraft
Δ	(relative) magnetic correction
d	wind direction
$\gamma = C_p/C_V$	heat capacity ratio
M	Mach number
p	pressure
ρ	air density
T	temperature
τ^-	descending temperature correction
τ^0	level flight temperature correction
τ^+	ascending temperature correction
v	wind speed
$\mathbf{v}$	wind vector
v_{rad}	radial wind speed
$\mathbf{v_a}$	air speed vector
v_a	air speed
v_g	ground speed
$\mathbf{v_g}$	ground track vector